Article

pubs.acs.org/Biomac

Self-Assembly Enhances the Strength of Fibers Made from Vimentin Intermediate Filament Proteins

Nicole Pinto,[†] Fei-Chi Yang,[‡] Atsuko Negishi,[†] Maikel C. Rheinstädter,[‡] Todd E. Gillis,*[,†,§] and Douglas S. Fudge*[,†,§]

[†]Department of Integrative Biology, University of Guelph, Guelph, Ontario N1G 2W1, Canada

[‡]Department of Physics and Astronomy, McMaster University, Hamilton, Ontario L8S 4M1, Canada

ABSTRACT: Hagfish slime threads were recently established as a promising biomimetic model for efforts to produce ecofriendly alternatives to petroleum polymers. Initial attempts to make fibers from solubilized slime thread proteins fell short of achieving the outstanding mechanics of native slime threads. Here we tested the hypothesis that the high strength and toughness of slime threads arise from the ability of constituent intermediate filaments to undergo a stress-induced α-to-β transition. To do this, we made fibers from human vimentin proteins that were first allowed to self-assemble into 10 nm intermediate filaments. Fibers made from assembled vimentin hydrogels underwent an α-to-β transition when strained and exhibited improved mechanical performance. Our data demonstrate that it is possible to make materials from intermediate filament hydrogels and that mimicking the secondary structure of native hagfish slime threads using intermediate filament self-assembly is a promising strategy for improving the mechanical performance of biomimetic protein materials.

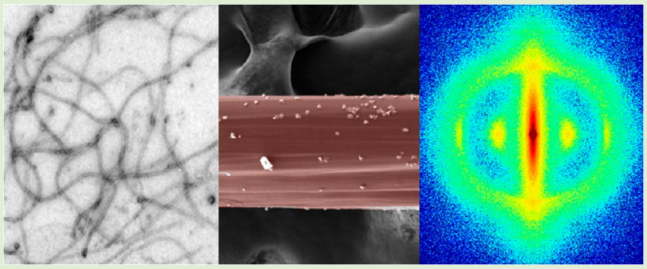

INTRODUCTION

Since the mid-1970s, petroleum prices have entered a phase of high volatility, which has spurred investment not only in alternative energy technologies but also in alternative materials that can be made without petroleum feedstocks. Natural fibers such as spider silks demonstrate that it is possible to produce high performance materials from sustainable feedstocks (i.e., protein) using aqueous chemistry.[1] In recent years, hagfish slime threads have emerged as a new biomimetic model for the production of fibrous protein materials with high strength and toughness.[2] Slime threads are a promising model because they are produced in the hagfish slime gland via mechanisms that may be easier to mimic than the complex mechanisms of silk spinning in spiders. Furthermore, they are built within cells from intermediate filament (IF) proteins, which are known to be able to self-assemble *in vitro* into 10 nm diameter filaments.

When hagfish are disturbed, they produce a slime that results from the mixing of products from two cell types in the slime glands: gland thread cells (GTCs) and gland mucous cells (GMCs).[3−5] GTCs each produce a single thread that is about 150 mm long in mature cells and 1−3 μm in diameter.[4,6,7] The thread is assembled from IF proteins α and γ, which have been classified as "keratin-like" because they possess all of the primary and secondary structural hallmarks of IFs.[8,9] A recent study found that draw-processed slime threads possess mechanical properties that rival spider dragline silk.[2] Negishi et al.[10] recently described a method by which fibers could be produced from formic acid solubilized hagfish slime thread proteins. The method involves pipetting a small volume of solubilized protein onto an electrolyte buffer and then drawing a fiber from the film that forms on the surface.[10] Fibers produced using this method possess mechanical properties that are inferior to native hagfish slime threads. The performance gap between native slime threads and these reconstituted fibers may be due to differences in protein structure and alignment. Native threads are produced from aligned bundles of IFs, whose structure is dominated by α-helical coiled-coils.[11] When slime threads are mechanically strained in water, the α-helices are extended, allowing for the formation of β-sheets and β-sheet crystallites, which endow the thread with high strength and toughness.[12] Negishi et al.[10] did not find evidence for coiled-coils or β-sheet crystallites in their fibers, nor any evidence that draw-processing of the fibers effects an $\alpha \rightarrow \beta$ transition as seen in native threads.

If native slime threads are stronger than those made from formic acid solubilized protein because of their ability to undergo an $\alpha \rightarrow \beta$ transition, we reasoned that it should be possible to boost the strength of artificial fibers by starting with proteins that possess some of the same structural characteristics within native threads. To do this, we made fibers from proteins that were first allowed to self-assemble into 10 nm diameter IFs. Our original intent was to assemble urea-solubilized hagfish slime thread proteins into IFs using a protocol published by Downing et al.[11] However, we (and others) have been unable to replicate filament assembly using their protocol or a number of variations on it (unpublished observations). We suspect that

Received: October 30, 2013
Revised: December 21, 2013
Published: December 23, 2013

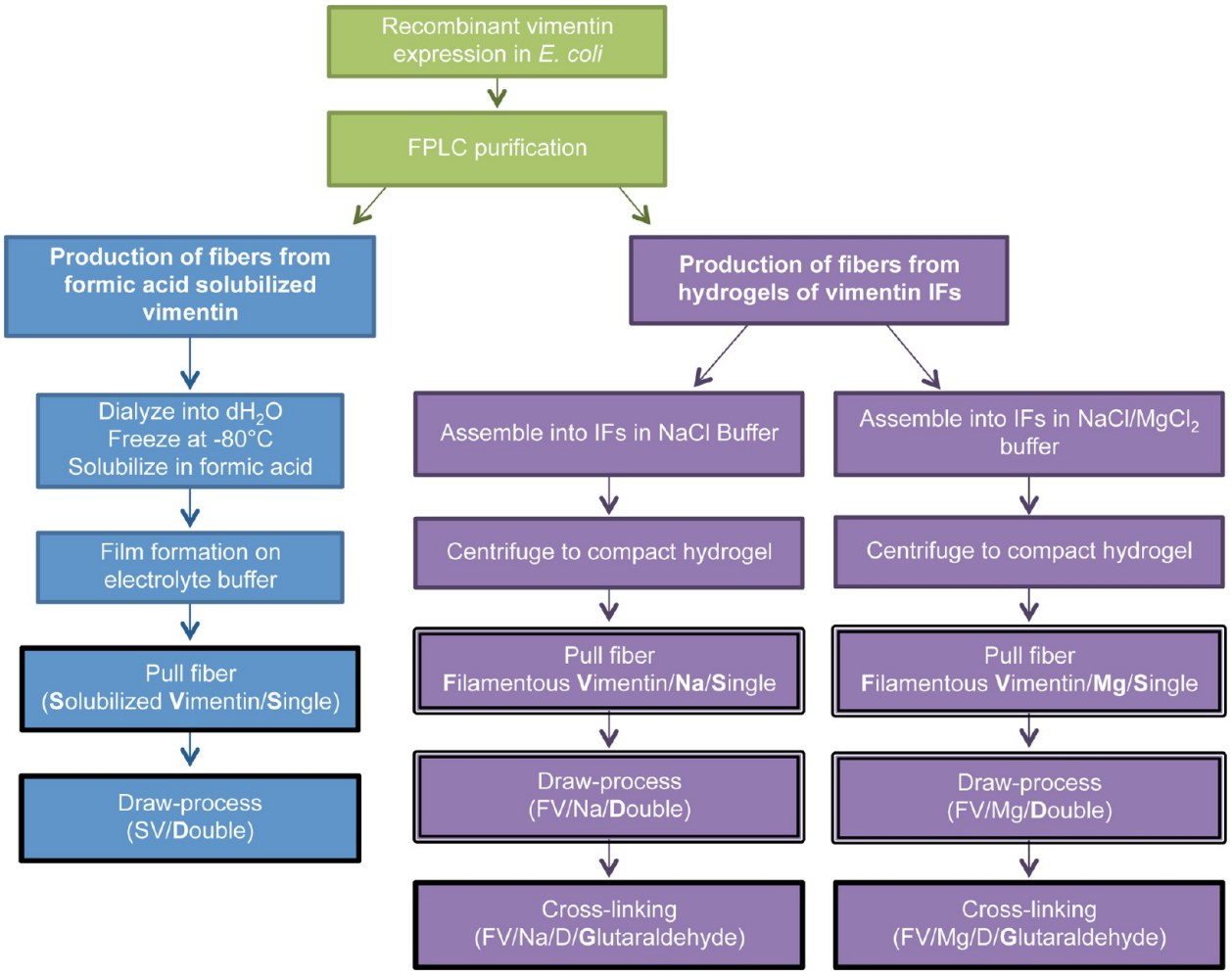

Figure 1. An overview of the two main methods used to make fibers from recombinant vimentin protein, using formic acid solubilized vimentin or hydrogels of assembled vimentin filaments. Boxes with a bold border denote the eight different fiber types that were characterized by tensile testing, and those with a double border also underwent structural analysis using wide-angle X-ray scattering (WAXS).

covalent modifications of thread proteins that occur during thread maturation[13] hinder the self-assembly process *in vitro*.

We therefore chose to work with an IF protein that has been intensively studied, the Type III IF protein, vimentin.[14,15] Human vimentin is a major cytoskeletal component of mesenchymal cells and is 54 kDa in size. This protein is also routinely made in research laboratories using recombinant bacteria, and detailed protocols exist for its self-assembly from urea-solubilized protein into networks of entangled high-aspect ratio IFs. Unlike hagfish slime thread IFs, which are heteropolymeric, vimentin IFs are homopolymeric, which further simplifies their production in the laboratory.

In the current study, we show that it is possible to make macroscopic materials from recombinant vimentin IFs, and we show that draw processing and Mg^{2+} cross-linking result in fibers with properties that are superior to previous attempts to make artificial materials from IF proteins. Structural data from WAXS experiments support the hypothesis that improvements in mechanical performance can be achieved by effecting an $\alpha \rightarrow \beta$ transition of IFs during draw processing.

MATERIALS AND METHODS

Protein expression. Recombinant vimentin was produced using a pDS5 plasmid containing the nucleotide sequence of the full-length human vimentin gene (NM_003380.3).[16] The plasmid was transformed into NovaBlue competent *E. coli* cells (Novagen, San Diego, CA, USA) using the standard protocol provided by the manufacturer. Using the High Pure Plasmid Isolation Kit (Roche Diagnostics, Indianapolis, IN, USA), plasmid DNA was purified and then sequenced to confirm the identity of the gene.

The pDS5 plasmid containing the vimentin cDNA was transformed into BL21-Gold(DE3) competent cells (Agilent Technologies, La Jolla, CA, USA) and grown on Luria–Bertani (LB) media agar containing 60 μg/mL carbenicillin. Growth plates were incubated overnight at 37 °C and the next day 100 mL of terrific broth (TB) containing 60 μg/mL carbenicillin was inoculated with 10 colonies from these plates. Cultures were agitated at 250 rpm at 37 °C overnight in an Excella E-25 Incubator Shaker (New Brunswick Scientific, Enfield, CT, USA).

Seven flasks containing 1 L of TB and carbenicillin (60 μg/mL) were inoculated with 10 mL of the overnight culture and shaken at 37 °C for 10 h until an optical density at 600 nm of approximately 1.8 was reached. These cells were harvested by centrifugation (6000 *g*) for 5 min at 4 °C. A sample from these pelleted cells was run on a 10% SDS-PAGE gel and then stained with Coomassie Brilliant blue G-250 (Bio-Rad, Hercules, CA, USA), which confirmed recombinant vimentin protein expression and accumulation in inclusion bodies. The pellet was solubilized using a series of seven buffers with sonication at each step.[17] The supernatant was stored at −20 °C.

Protein purification. Vimentin protein was purified on two consecutive columns using fast protein liquid chromatography (FPLC).[17,18] A fast flow diethylaminoethyl (FF DEAE) column was

dx.doi.org/10.1021/bm401600a | *Biomacromolecules* 2014, 15, 574−581

used first, with the vimentin protein diluted 10-fold using column running buffer (8 M urea, 5 mM Tris-HCl (pH 7.5), 1 mM EDTA, 0.1 mM EGTA, 1 mM DTT) (Herrmann and Aebi, 2004). Proteins bound to the column were eluted using an elution buffer (EB) consisting of the column running buffer plus 0.3 M KCl. The concentration of KCl running through the column was increased in six incremental steps by increasing the percentage of EB (11.5%, 15%, 21%, 31%, 37% and 100% EB). A fraction collector was used to collect all eluent and SDS-PAGE was used to determine the fractions containing the recombinant vimentin protein. The samples containing the target protein were pooled and then further purified using a carboxy methyl (CM) sepharose column using the same running and elution buffers. Pooled samples were dialyzed back into running buffer before they were applied to the CM column with a three-step elution gradient (11.5%, 33% and 100% EB). SDS-PAGE was used to identify the fraction containing the target protein as well as establish the purity of the samples. The fractions containing the target protein were pooled and stored at −20 °C with 10 mM methylammonium chloride (Herrmann et al., 2004).

Prior to filament assembly, the protein sample was thawed on ice and dialyzed (12−14 kDa MWCO)[17] against a series of buffers with decreasing urea concentrations (6, 4, 2 M urea in 5 mM Tris-HCl (pH 8.4), 1 mM DTT) at room temperature for 1 h each, followed by an additional dialysis against fresh buffer (5 mM Tris-HCl (pH 8.4), 1 mM DTT), which did not contain any urea, overnight at 4 °C. Aquacide II (EMD Millipore, Darmstadt, Germany) was used to concentrate the protein sample by removing about half of the initial volume of water. Changes in protein concentrations were measured using a Bradford assay and visualized using SDS-PAGE (Figure 2A).

Freeze-drying and solubilization in formic acid. Purified vimentin protein was dialyzed into dH_2O over three days with 3 dH_2O changes and lyophilized using a Virtis AdVantage freeze-dryer and stored at −80 °C. Freeze-dried samples (10% (w/v) protein concentration) were dissolved in 98% formic acid (Acros Organics, Geel, Belgium) and stirred in a closed container at room temperature for 3 h. The resulting solution was centrifuged at 17,000 *g* for 20 min. The white, unsolubilized pellet was discarded and the supernatant used immediately for fiber production.[10]

Fiber formation with formic acid solubilized vimentin. One μL of formic acid solubilized vimentin was applied to the surface of a 200 mM $MgCl_2$, 20 mM HEPES buffer (pH 7.5) solution.[10] After 20 s, a fiber was formed by drawing the resultant film using forceps and draping it over a 1 cm gap in a square of Nylon mesh (Figure 3A-D). Such fibers are referred to as the formic acid solubilized vimentin single-drawn fibers (SV/S) (Figure 1). When a subset of the fibers were dry, they were submerged in an aqueous 50% methanol solution for 5 min and stretched to approximately double their original length (from approximately 2 to 4 cm). These fibers are referred to as the formic acid solubilized vimentin double-drawn fibers (SV/D) (Figure 1).

Vimentin Filament Assembly and Fiber Formation from Hydrogels. Filament assembly was initiated by adding 500 μL of purified recombinant vimentin to an equal volume of NaCl assembly buffer (NAB), which consisted of 40 mM Tris-HCl (pH 7.0) and 200 mM NaCl. Full-length filaments were assembled at 37 °C for 1 h. Transmission electron microscopy (TEM) was used to visualize filaments during and immediately after assembly. For TEM, filament assembly was arrested with a buffer containing equal parts dialysis buffer (0 M urea) and NAB containing 0.2% glutaraldehyde (pH 7.5). TEM was carried out within 5 min of the addition of the 0.2% glutaraldehyde buffer.

For fiber formation, assembled vimentin filaments were centrifuged at 17000 *g* for 1 h to compact the hydrogel of entangled filaments, resulting in a visible gelatinous film on one side of the tube. Using a pipet tip, the edges of the film were lifted until it was possible to lift the whole film and pull it into a fiber. Fibers were air-dried overnight, and a subset of them was submerged in 50% aqueous methanol for 5 min and stretched between two pairs of forceps to an approximate strain of 50−100% and left to air-dry. Fibers made using this method are referred to as the filamentous vimentin single-drawn (FV/Na/S) and double-drawn (FV/Na/D) fibers. Noncovalent cross-linking was carried out by assembling filaments in an assembly buffer containing 16 mM Mg^{2+}, which has been shown to stiffen vimentin hydrogels.[19] Fibers made using this method are referred to as the filamentous vimentin Mg^{2+} single-drawn (FV/Mg/S) and double-drawn (FV/Mg/D) fibers (Figure 1).

A subset of the above double-drawn fibers was covalently cross-linked by exposing them to an aqueous 8% glutaraldehyde solution for 30 min, rinsing them with dH_2O, and allowing them to air-dry.[2] Fibers made using this method are referred to as FV/Na/D/G and FV/Mg/D/G fibers (Figure 1).

Material Properties of Vimentin Fibers. Fibers were mounted onto a cardstock paper frame and glued at both ends using Elmer's carpenter's wood glue. Fiber diameters and lengths were measured using a Nikon Eclipse 90i Epifluorescent microscope and NIS Elements AR v.6 software. Cross-sectional areas were calculated from diameters measured at 10 different locations evenly distributed along the length of the fiber. Tensile testing was performed using an Instron single column universal testing machine (model 3343; Instron, Norwood, Massachusetts, U.S.A.), with a 10 N load cell and a constant crosshead speed of 0.3 mm/min. Tests were performed at room temperature (23 °C) and at a relative humidity of 22−26%. Breaking stress (or "strength") was calculated as the engineering stress at failure, and breaking strain was calculated as the strain ($\Delta L/L_o$) at failure. Young's modulus was calculated as the slope of the stress/strain curve at the elastic region of the curve prior to the yield point. Strain energy at failure (or "toughness") was calculated by measuring the area under the stress/strain curve.

Scanning Electron Microscopy (SEM). Fibers were mounted onto SEM stubs using carbon tape and sputter coated using a Cressington model 108 auto system (final gold thickness ∼10 nm). SEM images of fibers were collected using an FEI Inspect S50 scanning electron microscope at an accelerating voltage of 20 kV with an aperture of 3.5 using an ETD secondary electron detector.

Transmission Electron Microscopy (TEM). IF assembly was confirmed by TEM using a LEO 912am TEM with a Cantega OSIS camera and iTEM software. Filament assembly was arrested with a buffer containing equal parts of dialysis buffer (0 M urea) in combination with NAB and 0.2% glutaraldehyde (pH 7.5), and visualization with TEM was carried out within 5 min of glutaraldehyde fixation. Negatively stained (2% uranyl acetate) whole mounts were placed on Formvar coated 200 mesh copper grids, and the TEM was operated at 100 kV.

X-ray Scattering. Two-dimensional X-ray diffraction patterns were recorded using the biological large angle diffraction experiment (BLADE) in the Laboratory for Membrane and Protein Dynamics at McMaster University. BLADE uses a 9 kW (45 kV, 200 mA) Cu Kα Rigaku Smartlab rotating anode at a wavelength of 1.5418 Å. Focusing multilayer optics provides a high intensity parallel beam with monochromatic X-ray intensities up to 10^{10} counts/(s·mm^2). A single fiber was selected and aligned parallel to the beam with typical slit settings of ∼100 μm (the diameter of the fibers, as listed in Tables 1 and 2) × 10 mm (along the fiber axis), and scattering signals in the equatorial plane and along the fiber axis were recorded.

Statistical Analysis. Statistical analyses were conducted using SigmaStat for Windows (v. 12.3). A two-way ANOVA was used to examine the main effects of draw-processing and assembly conditions, as well as the interaction between these two factors. Pairwise comparisons were done between treatments that differed in the level

Table 1. Summary of Mechanical Properties of SV Fibers[a]

fiber type	diameter (μm)	break stress (MPa)	break strain ($\Delta L/L_o$)
SV/S (8)	227.4 ± 18.0	3.4 ± 0.6	1.54 ± 0.1
SV/D (7)	65.4 ± 6.1*	68.5 ± 10.7*	0.4 ± 0.1*

[a]Asterisks (*) indicate significant differences between single and double drawn fibers according to a *t* test ($p < 0.05$). Sample sizes are indicated in parentheses. Values are mean ± standard error.

Table 2. Summary of Mechanical Properties of FV Fibers Showing the Effects of Assembly Buffer (Na vs Mg), Draw Processing (S vs D), and Cross-Linking with Glutaraldehyde (G)[a]

Fiber Type	Diameter (μm)	Break Stress (MPa)	Break Strain ($\Delta L/L_o$)	Young's Modulus (GPa)	Strain Energy (MJ/m^3)
FV/Na/S (13)	130.0 ± 10.6*†	50.5 ± 7.3§	0.8 ± 0.2	2.1 ± 0.6	14.9 ± 2.9
FV/Mg/S (14)	223.4 ± 13.8*‡	41.6 ± 4.8†	1.1 ± 0.2*	1.6 ± 0.5	18.9 ± 3.6§
FV/Na/D (9)	92.1 ± 7.6§†	95.5 ± 12.2*§	0.4 ± 0.1	2.2 ± 0.3	26.6 ± 6.1*
FV/Mg/D (11)	156.7 ± 14.7§‡	173.2 ± 15.4*†●	0.6 ± 0.1*	3.4 ± 0.3●	89.5 ± 18.8*§●
FV/Na/D/G (11)	105.5 ± 17.8	99.8 ± 9.8	0.4 ± 0.1	2.3 ± 0.3	31.9 ± 5.3
FV/Mg/D/G (12)	183.9 ± 18.0	94.3 ± 11.6●	0.4 ± 0.1	2.3 ± 0.2●	31.8 ± 5.6●

[a]In the top four rows, matching symbols (*, §, †, ‡) within the same column indicate significant differences from pairwise comparisons, which were made between treatments that differed in the level of one factor only (e.g., FV/Na/S vs FV/Na/D and FV/Na/S vs FV/Mg/S); treatments that differed in the level of two factors (e.g FV/Na/S vs FV/Mg/D) were not compared. In the bottom four rows, solid circles (●) indicate a significant difference between the glutaraldehyde cross-linked fiber and its un-cross-linked control (e.g., FV/Na/D/G vs FV/Na/D) according to a t test ($p < 0.05$). Sample sizes are indicated in parentheses. Values are mean ± standard error. A two-way ANOVA revealed significant main effects of assembly buffer ($p = 0.001$) and draw-processing ($p \ll 0.001$) on break stress

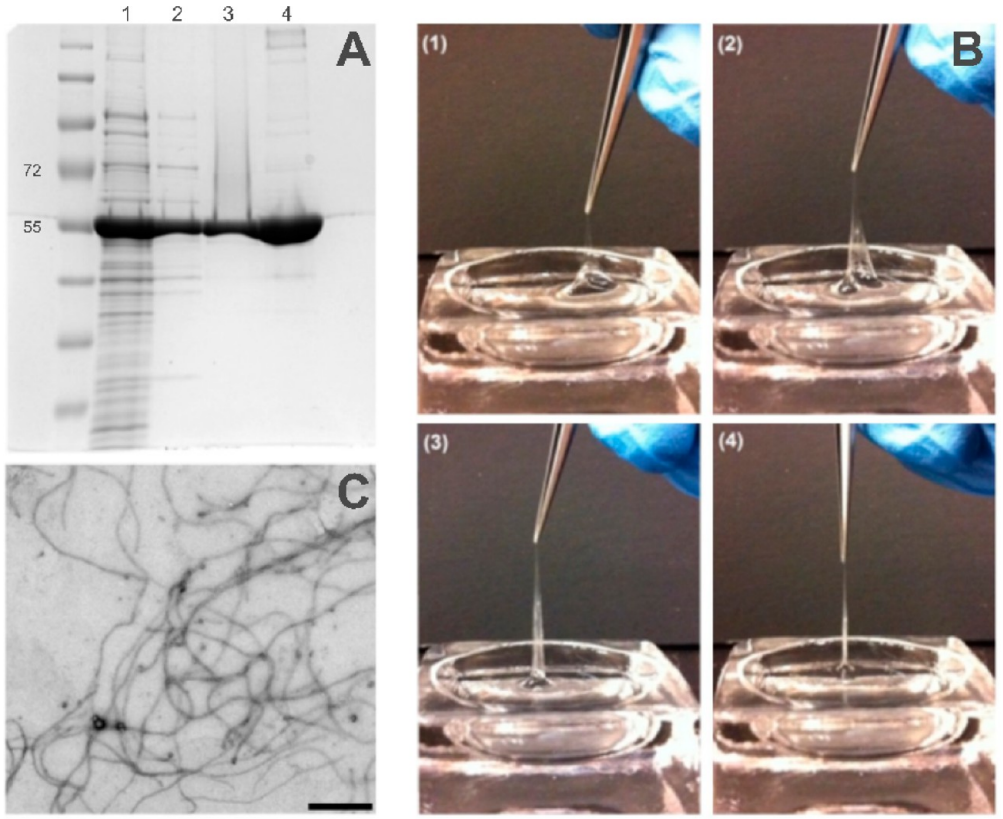

Figure 2. Vimentin purification and fiber and filament formation. (A) SDS-PAGE of proteins isolated from bacteria expressing recombinant vimentin. Left lane is mw ladder, (1) total protein, (2) after purification with FF DEAE column, (3) after purification with FF DEAE and CM sepharose columns, and (4) all purification steps plus Aquacide II to concentrate proteins. (B) SV fiber formation using the formic acid solubilized vimentin and methods from Negishi et al.[10] (C) FV fibers were made from vimentin proteins that were first allowed to self-assemble into 10 nm high aspect ratio IFs. Scale bar is 500 nm.

of a single factor only; pairwise comparisons of treatments that differed in levels of both factors were not made. The effects of glutaraldehyde were assessed by comparing data for cross-linked fibers with their respective un-cross-linked controls using t tests. A multiple linear regression was conducted in R (2.14.2) to simultaneously test for the effects of fiber diameter and assembly buffer (Na vs Mg) on the breaking stress of double-drawn fibers.

RESULTS

Fibers from Formic Acid Solubilized Vimentin Protein. Like solubilized hagfish slime thread proteins, formic acid solubilized vimentin formed a film on the surface of an electrolyte buffer, which could then be drawn into a fiber[10] (Figure 2B). SV fibers were weak (breaking stress 3.4 ± 0.6 MPa) ($n = 8$), although draw processing led to considerable increases in strength (68.6 ± 19.7 MPa, $n = 7$, $p = <0.001$) and a decrease in extensibility ($p = <0.001$) (Figure 4, Table 2).

Fibers from Hydrogels of Assembled Vimentin IFs. Vimentin filament assembly was temperature dependent, which is consistent with previous studies.[17] Assembly at room temperature yielded only short unit length filaments, whereas assembly at 37 °C yielded high aspect ratio mature vimentin IFs (Figure 2C). We were able to pull fibers from hydrogels of assembled vimentin IFs that were spun in a centrifuge to concentrate the filaments (Figure 3A,B). Double-drawing these

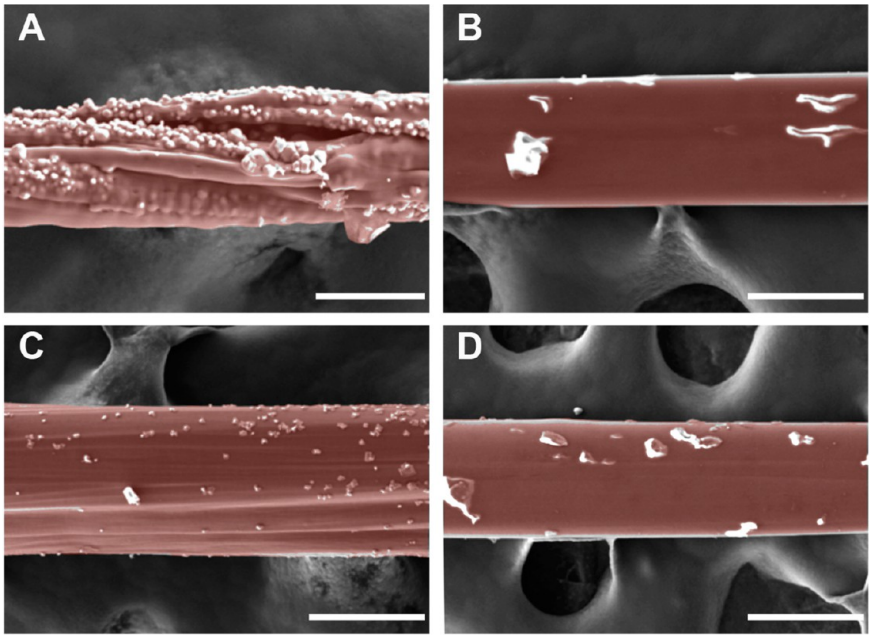

Figure 3. False color SEM images of FV fibers: (A) FV/Na/S fibers with salt crystals on surface; (B) FV/Na/D fibers; (C) FV/Mg/S fibers; (D) FV/Mg/D fibers. Top scale bars are 100 μm; bottom are 200 μm.

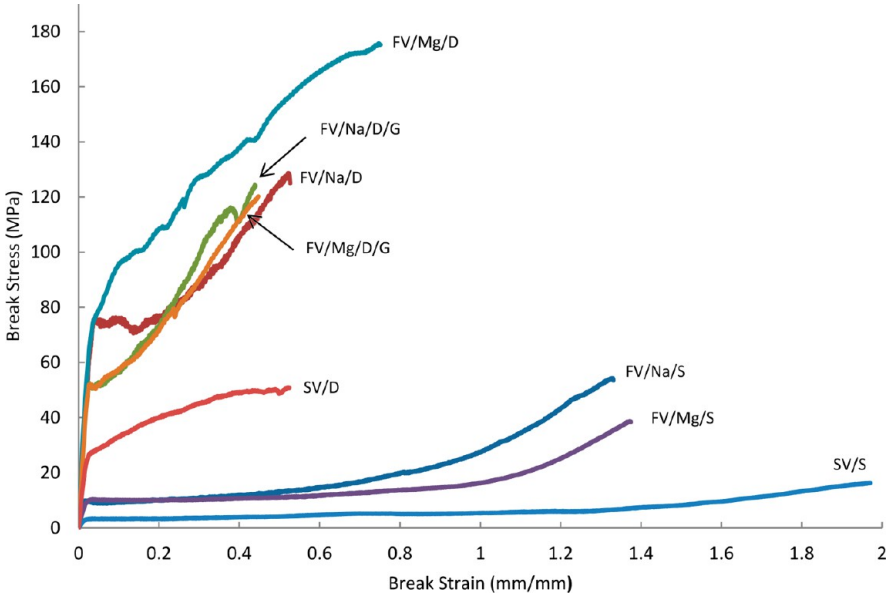

Figure 4. Representative stress−strain curves for fibers made using each of the eight vimentin assembly and processing conditions. SV/S fibers were the weakest; however draw processing led to large increases in stiffness and strength (SV/D). Draw processing of fibers made from vimentin IF hydrogels (FV/Na/S and FV/Mg/S) also led to large increases in stiffness and strength. Cross-linking with Mg^{2+} followed by draw-processing yielded the strongest and toughest fibers. Covalent cross-linking of draw-processed fibers did not improve fiber mechanics.

fibers in aqueous methanol and the inclusion of Mg^{2+} in the assembly buffer both resulted in fibers that were more uniform with a smoother surface (Figure 3C,D). Vimentin fibers made from filament hydrogels (FV) were stronger and stiffer than their single-drawn SV counterparts (p = <0.001). Assembly conditions (NaCl vs $MgCl_2$) and draw processing both had significant effects (p = <0.001) on FV fiber breaking strength, and the interaction between these two factors was also significant. The interactive effect was mainly a reflection of the relatively larger increase in break stress for fibers cross-linked with Mg^{2+} than those assembled and drawn in the absence of Mg^{2+}. FV/Mg/D fibers possessed the highest Young's modulus (3.4 ± 0.3 GPa), breaking stress (173.2 ± 15.4 MPa), and strain energy (89.5 ± 18.8 MPa) of all fiber treatments tested (Table 2). Treatment of FV/Na/D and FV/Mg/D fibers with glutaraldehyde did not lead to improved material properties and in the case of FV/Mg/D fibers, it made them weaker (Table 2, Figure 4).

Structural Properties of Fibers. WAXS patterns for FV/S fibers resembled those for other structures containing aligned IFs such as mammalian hard α-keratins and native hagfish slime threads. The main features of this pattern are a 9.6 Å (Figure 5A) and 9.5 Å (Figure 5C) equatorial reflection corresponding to the spacing between adjacent coiled-coils and a 5.0 Å (Figure

dx.doi.org/10.1021/bm401600a | *Biomacromolecules* 2014, 15, 574−581

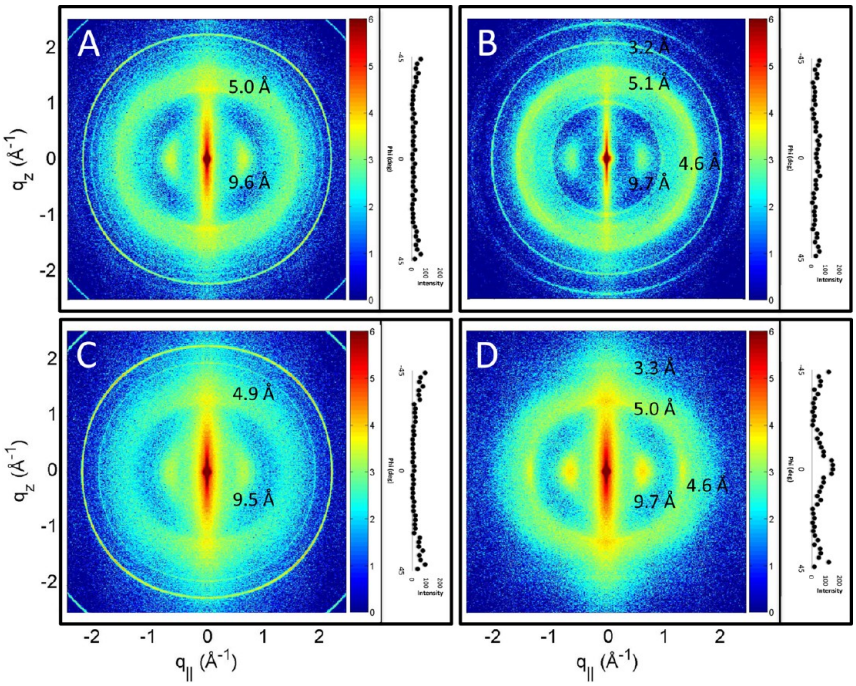

Figure 5. WAXS profiles for four kinds of FV fiber. (A) FV/Na/S and (C) FV/Mg/S fibers, which are both single-drawn, exhibited typical α-patterns, with equatorial peaks at 9.6 and 9.5 Å, respectively, and meridional peaks at 5.0 and 4.9 Å, respectively. Draw processed fibers, (B) FV/Na/D and (D) FV/Mg/D, had the same α-peaks as well as an equatorial peak at 4.6 Å, which corresponds to the spacing of protein chains within β-sheets. This peak was more prominent and well-defined in FV/Mg/D fibers than it was in FV/Na/D fibers. The insets show intensities along the azimuthal angle, phi, centered at the position of the 4.6 Å peak. No peak was observed in the single-drawn fibers in A and C.

5A) and 4.9 Å (Figure 5C) meridional reflection corresponding to the superhelical structure of α-helices twisting around each other within coiled-coils.[20] Draw processing of FV/Na/S fibers caused an increase in the sharpness of the aforementioned peaks in the resulting FV/Na/D fibers, indicating an increase in coiled-coil alignment and the subtle appearance of a 4.6 Å (Figure 5B) equatorial peak that likely denotes the spacing of protein chains within β-sheets (Figure 5). Draw processing of FV/Mg/S fibers resulted in the same coiled-coil pattern, plus a larger and sharper equatorial peak at 4.6 Å in the resulting FV/Mg/D fibers. These results suggest that it is possible to effect an α-to-β transition in macroscopic vimentin fibers, and that the process is more effective in the presence of a cross-linker such as Mg^{2+}.

DISCUSSION

Fibers from Formic Acid Solubilized Vimentin Protein. Negishi et al.[10] describe a method for making films and fibers from formic acid solubilized hagfish slime thread proteins at an air−electrolyte buffer interface. Here we show that this method can be used with solubilized vimentin protein. Observing this behavior in a Type III IF suggests that it may be an attribute of all IF proteins. Draw processing of SV fibers led to a large increase in breaking stress and a decrease in extensibility, but SV/D fibers were quite weak, even after draw processing, compared with native hagfish slime threads.

Fibers from Hydrogels of Vimentin IFs. We hypothesized that SV fibers are weak because they lack the structure of the IF proteins within native slime threads and therefore are unable to form β-sheets and β-sheet crystals, which are critical to the high strength of spider silks and hagfish slime threads.[12,21] Via centrifugation, we were able to concentrate vimentin IFs into a robust gel from which we could pull fibers. Stress−strain curves for FV fibers had a similar three-region shape (stiff Hookean region, long plateau, strain stiffening region) to curves reported for dry hagfish slime threads,[22] although the overall stresses were substantially lower (173 ± 15 MPa for FV/Mg/D fibers versus 530 ± 40 MPa for dry hagfish slime threads).[22] This suggests that the different kinds of IFs have similar dry mechanics and supports the idea that hagfish slime threads are a good model for understanding IF mechanics in general. Similarly, stress−strain curves for FV/D fibers resembled curves for draw-processed native slime threads, although again, with lower overall stresses. FV/Mg/D fibers were the strongest of all eight treatments, with strength values exceeding those from the best fibers made with reconstituted hagfish slime thread protein.[10]

Structural Considerations. X-ray diffraction scans of fibers made from formic acid solubilized hagfish slime thread proteins revealed no WAXS peaks.[10] In contrast FV/Na/S and FV/Mg/S fibers exhibited WAXS patterns similar to those seen in hard α-keratins like wool[23] and native slime threads.[12] These results demonstrate that we were able to achieve our goal of mimicking the secondary structure of proteins within hagfish slime threads. Furthermore, the improved mechanical performance of FV fibers is consistent with our hypothesis that protein structure is critical to the outstanding performance of hagfish slime threads. Draw processing of FV/Na/S and FV/Mg/S fibers led to an increase in the sharpness of WAXS peaks, indicating an increase in IF alignment, as well as the appearance of an equatorial peak at 4.6 Å, which corresponds to the spacing within β-sheets (Figure 5B,D). The mechanical stress-induced conversion of α-helices into β-sheets has been observed using WAXS in both keratin fibers[23,24] and hagfish slime threads[12] but never in a Type III IF. Others have demonstrated using atomic force microscopy that single IFs (including vimentin) can be

dx.doi.org/10.1021/bm401600a | Biomacromolecules 2014, 15, 574−581

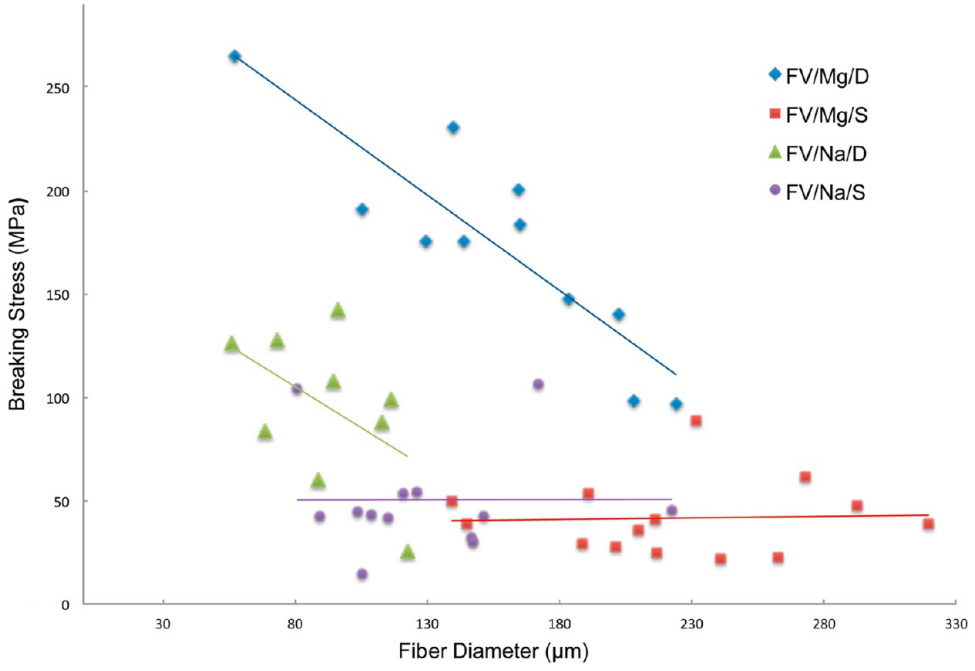

Figure 6. Fiber breaking stress plotted against diameter for four of the FV treatments. Strength was inversely proportional to diameter within FV/Na/D and FV/Mg/D fibers but had no effect on FV/Na/S and FV/Mg/S fibers. These data demonstrate that the superior mechanics of FV/Mg/D fibers are not driven by effects of Mg^{2+} on fiber diameter.

stretched to remarkable strains without breaking.[25,26] These stretching events lead to an obvious narrowing of the IFs that likely corresponds to an α-to-β transition, although WAXS measurements were not part of these experiments. The WAXS data presented in the current study demonstrate for the first time an α-to-β transition in a Type III IF.

Negishi et al.[10] found significant effects of various fiber spinning treatments on the mechanical properties of their fibers, but they also discovered that most of this variability could be understood as diameter effects. To test whether fiber diameter was the main driver of the treatment effects that we found (i.e., assembly conditions and draw processing), we plotted fiber strength against diameter for FV/Na/S, FV/Na/D, FV/Mg/S, and FV/Mg/D fibers (Figure 6). The data show that although diameter is a significant driver of mechanics within the double drawn fibers, the main effects of assembly conditions and draw processing are clearly not driven by effects of these variables on fiber diameter. This point is underscored by the fact that FV/Na/D fibers have smaller diameters than FV/Mg/D fibers (p = 0.002), and yet they are clearly weaker than the FV/Mg/D fibers. Fiber diameter is also important to consider when making comparisons with native hagfish slime threads. Extrapolation of the trend line for FV/Mg/D fiber strength vs diameter down to the size of native hagfish slime threads ($d \approx 1$ μm) yields a strength of about 317 MPa, which is almost half the strength of native threads (706 MPa).

Future Work. The data presented here demonstrate that it is possible to make robust fibers from IF hydrogels and that their mechanical properties are superior to fibers made from solubilized IF proteins. While the mechanical properties of these fibers are not yet outstanding, they are good enough to consider using them for biomedical applications such as artificial tendons (Table 3). Our data are consistent with the hypothesis that native slime threads owe their remarkable properties to the presence of β-sheets and β-sheet crystals, because vimentin fibers with the highest strength and toughness were also the ones with the highest β-sheet content. Despite the improvements in fiber mechanics that this study represents, there is a still a substantial performance gap between artificial IF fibers and hagfish slime threads (Table 3). Future work will focus on three strategies for bridging this gap. The first is to make finer fibers, as we have shown that diameter is an important determinant of mechanics in double drawn fibers. Another strategy is to effect a more complete α-to-β transition. Draw-processed slime threads exhibit a much stronger 4.6 Å equatorial peak than FV/D fibers.[12] Creating more β-sheet

Table 3. Summary of the Mechanical Properties of Various Protein-Based Fibers and Fibers Produced from Each of the Assembly Conditions Tested in This Study

material	break stress (MPa)	break strain (mm/mm)	Young's modulus (GPa)
amyloid protein nanofiber[27]	326		14
recombinant honeybee silk protein[28]	150	0.5	
native spider silk[29]	800−1400	0.2−0.3	
recombinant spider silk protein[30]	508	0.2	21
hagfish slime thread, dry[2]	467	1.2	9
hagfish slime thread, stretched, dry[2]	706	0.4	8
regenerated hagfish slime thread[10]	150	0.2	4
human patellar tendon[31]	65	0.14	0.66
FV/Na/S	51	0.8	2.1
FV/Na/D	96	0.4	2.2
FV/Na/D/G	100	0.4	2.3
FV/Mg/S	42	1.1	1.6
FV/Mg/D	173	0.6	3.4
FV/Mg/D/G	94	0.4	2.3
SV/S	3	1.5	
SV/D	69	0.4	

dx.doi.org/10.1021/bm401600a | Biomacromolecules 2014, 15, 574−581

structure should further increase strength and stiffness. We will also look to the hagfish slime thread model as a source of inspiration for improving the mechanics of IF-based materials. In particular, we will continue to study the mechanisms of slime thread formation from IF proteins within the cytoplasm of hagfish gland thread cells.

CONCLUSION

In this study, we have developed a method for producing fibers made from self-assembled vimentin IFs. We have also shown for the first time that 10 nm filaments assembled *in vitro* undergo an $\alpha \rightarrow \beta$ transition when strained, suggesting that 10 nm IFs in cells could potentially undergo this same transition. From all of the assembly conditions, fibers that were cross-linked with Mg^{2+} exhibited the strongest mechanical properties. Overall, this study, using novel methods to produce fibers from hydrogels of 10 nm IFs, opens up new possibilities for the production of protein-based fibers. The production of high-performance protein polymers from such fibers has the potential to decrease our reliance on petroleum-based synthetics.

AUTHOR INFORMATION

Corresponding Authors

*Tel: 519-824-4120 (ext. 58786). Fax: 519-767-1656. E-mail: tgillis@uoguelph.ca.

*Tel: 519-824-4120 (ext. 56418). Fax: 519-767-1656. E-mail: dfudge@uoguelph.ca.

Author Contributions

§Co-senior authors.

Notes

The authors declare no competing financial interest.

ACKNOWLEDGMENTS

We thank Dr. Harald Herrmann for the pDS5 plasmid and Laurent Kreplak for assistance with vimentin assembly. Thanks also to Bob Harris of the Electron Microscopy Unit at the University of Guelph and Jean-Luc Stiles for help with statistics. This work was supported by NSERC Discovery and Accelerator grants and Ontario Early Researcher Awards to DF, NSERC Discovery, Canadian Foundation for Innovation (CFI), Ontario Ministry of Economical Development and Innovation, and Ontario Early Researcher Awards to M.C.R., and NSERC Discovery and Research Tools and Instrumentation grants to T.G.

REFERENCES

(1) Shao, Z.; Vollrath, F.; Yang, Y.; Thøgersen, H. C. *Macromolecules* **2003**, *36*, 1157−1161.

(2) Fudge, D. S.; Hillis, S.; Levy, N.; Gosline, J. M. *Bioinspiration Biomimetics* **2010**, *5*, 1−8.

(3) Newby, W. W. *J. Morphol.* **1946**, *78*, 397−409.

(4) Fernholm, B. *Acta Zool.* **1981**, *62*, 137−145.

(5) Spitzer, R. H.; Downing, S. W.; Koch, E. A.; Salo, W. L.; Saidel, L. J. *J. Cell Biol.* **1984**, *98*, 670−677.

(6) Downing, S. W.; Spitzer, R. H.; Koch, E. A.; Salo, W. L. *J. Cell Biol.* **1984**, *98*, 653−669.

(7) Fudge, D. S.; Levy, N.; Chiu, S.; Gosline, J. M. *J. Exp. Biol.* **2005**, *208*, 4613−4625.

(8) Koch, E. A.; Spitzer, R. H.; Pithawalla, R. B.; Parry, D. A. *J. Cell Sci.* **1994**, *107*, 3133−3144.

(9) Koch, E. A.; Spitzer, R. H.; Pithawalla, R. B.; Castillos, F. A., III; Parry, D. A. *Int. J. Biol. Macromol.* **1995**, *17*, 282−292.

(10) Negishi, A.; Armstrong, C. L.; Kreplak, L.; Rheinstadter, M. C.; Lim, L. T.; Gillis, T. E.; Fudge, D. S. *Biomacromolecules* **2012**, *13*, 3475−3482.

(11) Downing, S. W.; Spitzer, R. H.; Koch, E. A.; Salo, W. L. *J. Cell Biol.* **1984**, *98*, 653−669.

(12) Fudge, D. S.; Gardner, K. H.; Forsyth, V. T.; Riekel, C.; Gosline, J. M. *Biophys. J.* **2003**, *85*, 2015−2027.

(13) Spitzer, R. H.; Koch, E. A.; Downing, S. W. *Cell Motil. Cytoskeleton* **1988**, *11*, 31−45.

(14) Qin, Z.; Kreplak, L.; Buehler, M. J. *PLoS One* **2009**, *4*, No. e7294.

(15) Herrmann, H.; Häner, M.; Brettel, M.; Müller, S. A.; Goldie, K. N.; Fedtke, B.; Lustig, A.; Franke, W. W.; Aebi, U. *J. Mol. Biol.* **1996**, *264*, 933−953.

(16) Bujard, H.; Gentz, R.; Lanzer, M.; Stueber, D.; Mueller, M.; Ibrahimi, I.; Haeuptle, M. T.; Dobberstein, B. *Methods Enzymol.* **1987**, *155*, 416−433.

(17) Herrmann, H.; Kreplak, L.; Aebi, U. *Methods Cell Biol.* **2004**, *78*, 3−24.

(18) Herrmann, H.; Aebi, U. *Annu. Rev. Biochem.* **2004**, *73*, 749−789.

(19) Lin, Y.-C.; Broedersz, C. P.; Rowat, A. C.; Wedig, T.; Herrmann, H.; MacKintosh, F. C.; Weitz, D. A. *J. Mol. Biol.* **2010**, *399*, 637−644.

(20) Crick, F. H. C. *Nature* **1952**, *170*, 882−883.

(21) Gosline, J. M.; DeMont, M. E.; Denny, M. W. *Endeavour* **1986**, *10*, 37−43.

(22) Fudge, D. S.; Gosline, J. M. *Proc. R. Soc. London, Ser. B* **2004**, *271*, 291−299.

(23) Kreplak, L.; Doucet, J.; Dumas, P.; Briki, F. *Biophys. J.* **2004**, *87*, 640−647.

(24) Kreplak, L.; Franbourg, A.; Briki, F.; Leroy, F.; Dalle, D.; Doucet, J. *Biophys. J.* **2002**, *82*, 2265−2274.

(25) Guzmán, C.; Jeney, S.; Kreplak, L.; Kasas, S.; Kulik, A. J.; Aebi, U.; Forró, L. *J. Mol. Biol.* **2006**, *360*, 623−630.

(26) Kreplak, L.; Herrmann, H.; Aebi, U. *Biophys. J.* **2008**, *94*, 2790−2799.

(27) Meier, C.; Welland, M. E. *Biomacromolecules* **2011**, *12*, 3453−3459.

(28) Weisman, S.; Haritos, V. S.; Church, J. S.; Huson, M. G.; Mudie, S. T.; Rodgers, A. J. W.; Dumsdat, G. J.; Sutherland, T. D. *Biomaterials* **2010**, *31*, 2695−2700.

(29) Shao, Z.; Vollrath, F. *Polymer* **1999**, *40*, 1799−1806.

(30) Xia, X. X.; Qian, Z. G.; Ki, C. S.; Park, Y. H.; Kaplan, D. L.; Lee, S. Y. *Proc. Natl. Acad. Sci. U.S.A.* **2010**, *107*, 14059−14063.

(31) Johnson, G. A.; Tramaglini, D. M.; Levine, R. E.; Ohno, K.; Choi, N. Y.; Woo, S. L. *J. Orthop. Res.* **1994**, *12*, 796−803.